FINAL TECHNICAL REPORT
1998 January 20

TITLE: Stellar Occultation Studies of the Solar System
GRANT NUMBER: NAG2-1085
STARTING AND ENDING DATES: 1996 April 1 through 1997 September 30
PRINCIPAL INVESTIGATOR: James L. Elliot
GRANTEE:

Lowell Observatory
1400 West Mars Hill Road
Flagstaff, Arizona 86001

This document constitutes the Final Technical Report for NASA Ames Grant NAG2-1085 to Lowell Observatory.

ABSTRACT

Earth-based observations of stellar occultations provide extremely high spatial resolution for bodies in the outer solar system--about 10,000 times better than that of traditional imaging observations. Stellar occultation data can be used to establish the structure of atmospheres and rings of solar system bodies at high spatial resolution. Airborne occultation observations are particularly effective, since the controlled mobility of the observing platform allows the observer to fly within the optimum part of the occultation shadow for most events that are visible from Earth. Airborne observations are carried out above any clouds and are nearly free of scintillation noise from the Earth's atmosphere. KAO occultation observations resulted in the first detection of gravity waves in the Martian atmosphere, discovery of the Uranian rings, the first detection of Pluto's atmosphere, the first Earth-based investigations of Triton's atmosphere, and the discovery of narrow jets from Chiron's nucleus. The first SOFIA occultation opportunity will be an investigation of Pluto's atmospheric structure in November, 2002, and will resolve a problem that has lingered since the KAO discovery observation fourteen years earlier.

We plan to continue our successful airborne occultation program with the greatly enhanced capability provided by SOFIA. We propose here to replace our KAO occultation photometer with one having twice the throughput, half the noise, a somewhat wider wavelength range, four times the field of view, and ten times the frame rate to optimize its performance and to capitalize on the larger collecting area offered by SOFIA. It will also allow for simultaneous visible and IR occultation observations, greatly enriching the results that we can obtain from occultations. We call this new imaging occultation photometer HOPI (High-speed Occultation Photometer and Imager). HOPI will provide a signal-to-noise ratio two to four times that of our present photometer for a given event, will permit useful observations of the more numerous events involving fainter stars, and will allow higher time resolution observations to be made. HOPI's characteristics also make it an ideal instrument for initial and ongoing evaluations of the SOFIA telescope's performance.

TABLE OF CONTENTS

I. THE OCCULTATION TECHNIQUE

Stellar occultations by solar system bodies have emerged from being an infrequent "astronomical happening" in the earlier parts of this century to a routine tool used by a growing number of planetary astronomers in the 1980s and 1990s. The increasing popularity of the technique has been due to (i) the 10,000-fold improvement in spatial resolution that it affords over ordinary ground-based methods for probing the outer solar system, (ii) the probing of transmission and refraction properties of dust and atmospheres—providing complementary information to the reflection and emission data obtained by other methods, (iii) several technical advancements that have allowed occultations to be observed more frequently and with continually improving signal-to-noise ratios, and (iv) improvements in the astrometric methods used to accurately predict where occultations will be visible. Prominent among the technical advancements has been our use of the KAO as a mobile occultation observatory, beginning in 1976 with the ε Geminorum occultation by Mars.

Even with interferometry, a baseline greater than *one kilometer* would be required to achieve the equivalent spatial resolution afforded by stellar occultations for outer solar system bodies at a wavelength of 0.75 μm! High spatial resolution is achieved with the occultation technique because the distant occulting body is not imaged *per se*. Hence the attendant problems of seeing do not enter in. Instead, we are probing with starlight that is refracted, absorbed, or diffracted at the occulting body before the light reaches the Earth's atmosphere. As a result, the spatial resolution of our occultation observations is limited by some combination of (i) Fresnel diffraction, (ii) the angular diameter of the occulted star, (iii) the time resolution of the data recording, and (iv) the signal-to-noise ratio of the data. Seeing and Fraunhofer diffraction effects by the telescope used to collect the starlight do not directly affect the spatial resolution for probing the occulting body—they affect the resolution only through their effect on the signal-to-noise ratio of the data.

Observation of a stellar occultation requires recording the starlight as a function of time, while the relative motion of the observer and the occulting body produces a "line scan" of stellar intensity as a function of position on the occulting body. If observations can be carried out simultaneously from more than one telescope, we then have multiple line scans across the occulting body, which give us two-dimensional information. Depending on the physical characteristics of the occulting body, the line scan can be a trace of optical depth through ring material, a probe of the differential refraction produced by an atmosphere, or just an "on-off" event that gives us the length of a chord across an asteroid or small satellite. Relating the intensity trace to an accurate time base is critical, since the time tag on each stellar intensity point is directly related to a position on the occulting body.

It is not surprising that such a powerful observational tool has been used for some exciting work. Major results from the occultation technique include: the first observations of thermal waves in the Martian atmosphere; the discovery and comprehensive study of the Uranian ring system; the accurate measurement of the sizes and shapes of several asteroids; the discovery of waves and other features in the Saturnian rings; the probing of the upper atmospheres of the giant planets; the discovery of the Neptune ring-arcs; the detection of a tenuous atmosphere surrounding Pluto; the discovery of narrow jets emanating from the nucleus of Chiron; and most recently, the first direct probe of Triton's atmosphere since the Voyager encounter in 1989. KAO results have been definitive in much of this work. With SOFIA and our proposed High-speed Occultation Photometer and Imager (HOPI), we anticipate many more exciting results.

II. OBJECTIVES FOR AIRBORNE OCCULTATION OBSERVATIONS

In this section we describe our occultation objectives for SOFIA and our proposed high-speed occultation photometer, HOPI. The successful execution of these programs depends critically on

the ability to place SOFIA near the center of the occultation shadow-paths and on the enhanced sensitivity and speed of HOPI over our present occultation photometer, PCCD. To aid in comparison of different occultations, we use the symbol "S/N" throughout this section to mean the ratio of the unocculted stellar signal to the rms noise on the occultation curve for an integration time corresponding to a 10 km motion of the occultation shadow (0.5 sec integration with v = 20 km/s).

TRITON'S VARIABLE ATMOSPHERE

COMPARISON OF TRITON AND PLUTO

Triton and Pluto, two bodies that likely formed in the solar nebula (rather than a pre-planetary nebula), hold the promise of telling us much about early conditions in the outer solar system. Triton and Pluto are remarkably similar in size and density, and each suffered an early catastrophic event: Triton's retrograde orbit indicates that it was captured by Neptune in the early history of the solar system (Goldreich et al. 1989), while Pluto's binding with Charon also required a large dissipation of energy (McKinnon 1989). The low probability of such events for two isolated bodies implies that Triton and Pluto may be representatives of a large number of such bodies that existed in the past—perhaps remnants of the building blocks for the larger planets. Support for this idea comes from the discovery of a several trans-Neptunian bodies (Jewitt & Luu 1993), from which a present population of 3.5×10^4 bodies (termed Kuiper Belt objects) larger than 100 km and 30-50 AU from the sun has been inferred (Jewitt & Luu 1995).

The tenuous atmospheres of Triton and Pluto are similar in that the major constituent of each is N_2, although Pluto's atmosphere has considerably more CH_4 than does Triton's (Spencer, Buie, & Bjoraker 1990). Since these atmospheres are presumed to be in vapor pressure equilibrium with surface ices, large seasonal changes in surface pressure have been predicted for each (Trafton 1990; Hansen & Paige 1992; Spencer & Moore 1992). Hence, the understanding of the mechanisms at work in each of these atmospheres requires probing them throughout a seasonal cycle—Triton: 600 years; Pluto: 240 years.

Before we can understand how changes occur in these atmospheres, we must understand their basic physical state now: how the interaction of solar radiation with the atmospheric constituents and exchanges of material between the atmospheres and surface ices affect the atmospheric structure. Models have been constructed for both atmospheres (Yelle, Lunine, & Hunten 1991; Stansberry et al. 1992; Lellouch 1994; Stansberry et al. 1994; Strobel & Summers 1995; Strobel et al. 1996), and the latest one (Strobel et al. 1996) applies the same physical processes and calculation methods to each body, with the large observed differences in the atmospheric structures being solely due to differences in the abundances of minor constituents (CH_4, CO, HCN) and the boundary conditions (heat flow from above due to magnetospheric electron heating and the surface temperature). In a companion KAO analysis proposal, we propose to test the validity of the model for Pluto and Triton through further analysis of three occultation light curves obtained for these bodies with CCD photometers on the KAO: two occultation light curves for Triton (1993 July, 1995 August) and one for Pluto (1988 June). The same physical model applies to both atmospheres and we have the same type of occultation data for both, so our work provides precise comparisons between the two atmospheres.

PRESENT KNOWLEDGE

Triton's atmosphere has been probed by several instruments aboard the Voyager 2 spacecraft in 1989, and by KAO observations of a stellar occultation in 1993, and KAO and ground-based observations of stellar occultations in 1995. First we discuss the results from three Voyager instruments: (1) the Imaging Science Subsystem (ISS), (2) the Ultraviolet Spectrometer (UVS) and (3) the Radio Science Subsystem (RSS). Each of these instruments investigated a different region of the atmosphere and was sensitive to different properties. Aeolian features noted on images of the surface have been used to define the pattern of surface winds, while the remarkable "plumes" trace wind speeds up to an altitude of 8 km, where the troposphere ends (Smith et al. 1989). Several hypotheses have been advanced to explain the plumes: dust devils (Ingersoll & Tryka

1990), buoyant columns (Smith et al. 1989; Yelle et al. 1991), and geysers (Soderblom et al. 1990).

The RSS measures the phase and amplitude at two wavelengths, being sensitive to both the ionized and neutral atmospheric components. RSS found a high electron density at 400 km altitude (implying the presence of an ionizing heat source) and detected the neutral atmosphere near the surface (Tyler et al. 1989). However, because the surface pressure of Triton reported by Tyler et al (1989) is only about 14 μbar, the phase shift of the radio signal never reaches 2 radians, and these results are not considered as reliable as what has been obtained from RSS occultations at millibar pressures. Profiles of the lower atmospheric structure in 1989 inferred from the RSS data alone have been presented (Tyler et al. 1989), and a physical model based on RSS and UVS results has been derived (Strobel & Summers 1995; Strobel et al. 1996).

The UVS measurements of spectra and occultations were in the range 500-1700 Å (Broadfoot et al. 1989; Yelle et al. 1991). From the spectral data, N_2 and NII were detected, and from the UVS occultation data, strict limits were placed on the amount of CO. The [CO]/[N_2] ratio is less than one percent, so Triton's atmosphere is almost purely N_2. From the solar occultation, a number density for N_2 is derived near 600 km where there was appreciable extinction of wavelengths corresponding to the N_2 ionization continuum. Similarly, CH_4 was detected at an altitude of 40 km where there was extinction of the longer wavelengths in the solar occultation data. From the solar occultation data, a temperature of 95K in the 500 to 700 km range is determined from the measured N_2 density profile and an assumption of hydrostatic equilibrium.

From the state of Triton's atmosphere derived from the Voyager data, variability with season has been inferred by modeling how insolation affects surface ices (Hansen & Paige 1992; Spencer & Moore 1992). Some models predict extremely large changes in surface pressure (Fig. 1), while other models predict less. Earth-based observations of changes in the disk-integrated properties between 1977-89, show that significant seasonal changes do occur (Cruikshank et al. 1989). The free parameters in the models are thermal inertia, surface albedo, frost albedo, frost emissivity, and the N_2 inventory. Since the least well-determined of these are the thermal inertia and N_2 inventory, the characterization of the volatile cycles through determination of the changes in atmospheric pressure would give us information about these quantities.

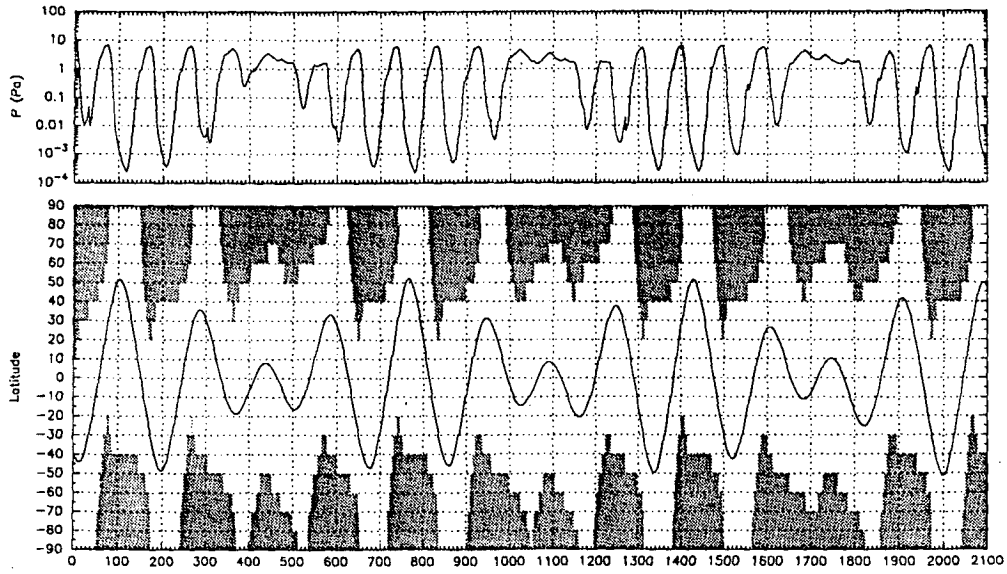

Figure 1. A possible scenario for Triton's surface pressure (upper panel) and latitude of subsolar point, with frost deposits (lower panel). This model predicts that the surface pressure is dropping by about 8% per year in 1995, so that the surface pressure at the time of the Tr148 occultation would have been about 48% less than that during the Voyager encounter (about 7 μbar now). Other models predict different pressure changes. The horizontal axis in this figure is in years AD. (after Hansen and Paige 1992)

One way to determine the extent of seasonal variability of Triton's atmosphere is through observation of a series of stellar occultations, which we began with the KAO observation of the Tr60 occultation in 1993 July (Elliot, Dunham, & Olkin 1993; Olkin et al. 1993) and followed up with the observation of an occultation of Tr148 in 1995 August with the KAO (Olkin et al. 1995)

and ground-based stations (Dunham et al. 1995; Olkin et al. 1995; Reitsema et al. 1995; Wasserman, Buie, & Millis 1995).

As a first-order analysis, these data have been fit with isothermal models (Elliot & Young 1992),. This is useful for comparative analyses, such as determining changes in atmospheric pressure from one occultation to the next, even though an isothermal model is not an accurate representation of the structure of Triton's upper atmosphere. Although the Voyager RSS occultation probed to the surface, the deepest altitude probed by any of the occultation chords at the center of the light curve is just below 1370 km, with the most accurate determination of pressure at about 1400 km. The KAO data probe well above levels of significant haze in Triton's atmosphere (Hillier & Veverka 1994), so extinction was not included in the fitted models.

In Fig. 2, we have plotted the pressure for the KAO results at 1400 km, along with the surface-pressure measurement for the Voyager RSS occultation. Using only the stellar occultation data, so that there is no need to depend on an atmospheric model for comparison, we find that the pressure at 1400 km decreased by 0.20 ± 0.14 μbar between 1993 & 1995 ($-6\% \pm 4\%$/yr); significant at only the 1.5σ level, this result is best interpreted as an upper limit on any pressure changes.

Since the stellar occultations and the RSS refer to different altitudes on Triton, we have compared them by plotting the model of Strobel et al (1996), which uses the RSS data point as a boundary condition. The dashed lines in Fig. 2 show the uncertainties in the pressure profile due to the $\pm 1\sigma$ error in the surface radius, as determined by Voyager. The KAO measurements indicate somewhat higher pressures at 1400 km than one would infer from the Voyager measurement in 1989, as extrapolated to 1400 km with the Strobel et al (1996) model. Taken at face value, we see the stellar occultation points lie well above the model pressure, indicating a significant difference between the Voyager RSS results and the stellar occultation results. Three interpretations of the difference between the stellar occultation results and the extrapolated Voyager surface pressure are possible: (i) Triton's surface pressure substantially increased between the times of the Voyager encounter and the stellar occultations, (ii) the surface radius of Triton is about 1360 km instead of 1352 km, or (iii) the Strobel et al (1996) model used to connect the RSS and stellar occultation measurements is not an accurate description of Triton's atmospheric structure.

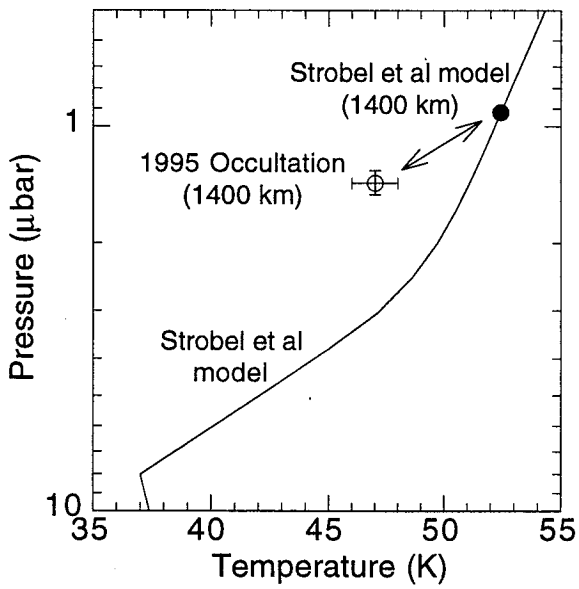

Figure 2. Triton's lower atmosphere. The solid line represents the model of Strobel *et al.* (1996), with the solid point on the line being the state of Triton's atmosphere predicted by the model (based on 1989 Voyager data) at a radius of 1400 km. The open circle with error bars represents a weighted average of the 1995 occultation results (Olkin et al. 1997). Since the data and model should agree in both temperature and pressure, the double-headed arrow shows the magnitude of disagreement, which is much too great to be explained by the error bars. More data are needed in order to determine whether the difference represents a change in atmospheric structure between 1989 and 1995, or a poor representation of the state of the atmosphere by the model.

Clearly we need a longer series of occultation observations than just the 1993 and 1995 events, and it would be helpful for comparison with the 1989 Voyager results if we could find an accurate surface radius for Triton (since the Voyager surface pressure refers to the surface radius, and this has an error bar of 5-10 km). The step due to the surface occultation would be in the far-limb flux

and amount to only a 0.5% drop, so we would need an event of high S/N to detect it. We also note that we have been unable to detect the light-curve "spikes" (Elliot & Veverka 1976), which are indicative of atmospheric waves or turbulence. We would like to learn whether the light curves are devoid of spikes because Triton's atmosphere is much more stable than those of the gas giants, whose occultation light curves contain many of these features, or whether we have just not detected the spikes because the time resolution of our PCCD is inadequate.

PROPOSED OBJECTIVES

The objectives below may be achieved with the same occultations, depending on the particulars of the events. All Triton occultation observations should be carried out as nearly as possible to a central chord, in order to probe most deeply into the atmosphere and to be able to use the central flash for accurate astrometry to determine the closest approach distance to the center of the shadow.

1) Detect or put a stringent upper limit on the variability of Triton's atmospheric structure by probing its atmosphere with a stellar occultation observation with S/N $\geq$ 50 once every 1-2 years.

2) Establish Triton's surface radius by detecting the limb occultation with an event that has S/N $\geq$ 250. Because the limb signature will be in the far-limb flux, long averaging times may be used to increase S/N.

3) Characterize the latitudinal and seasonal properties of Triton's atmospheric hazes (Hillier & Veverka 1994) by observing occultations simultaneously in the visible and IR with S/N $\geq$ 250. These would also appear in the slowly varying far-limb flux, allowing long averaging times to be used to maximize the S/N.

4) Search for non-isothermal structures in Triton's atmosphere by observing an occultation with a time resolution of 0.05 s.

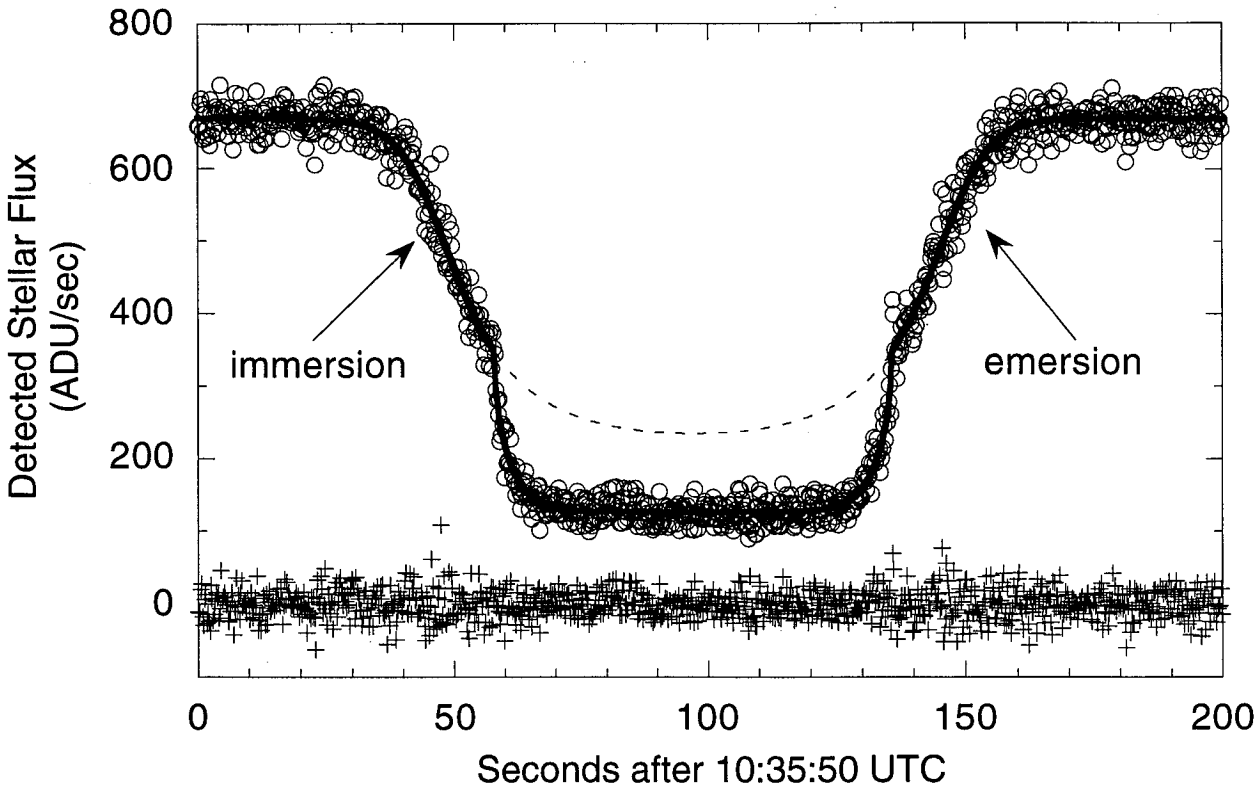

Figure 3. Pluto occultation light curve from the KAO. The gradual decrease in the starlight is due to Pluto's atmosphere. Just below half intensity, the starlight drops more abruptly, indicating either an extinction layer or sharp thermal gradient in Pluto's atmosphere. An isothermal-temperature model that fits the upper atmosphere is indicated by the dashed line. The solid-line model includes extinction, and the residuals from this fitted model are shown along the bottom. For reference, this light curve has S/N = 46 for a 10 km shadow motion (or about 113 over the middle atmosphere scale height of 60 km) (From Elliot & Young 1992.)

DOES PLUTO HAVE A HAZE LAYER?

Attempts to observe a stellar occultation by Pluto date back to 1965 (Halliday 1965), but the first definitive observations of a stellar occultation occurred in 1988. This occultation was recorded by seven ground stations in New Zealand and Australia (Millis et al. 1993), but the KAO provided the light curve with the best S/N (Elliot et al. 1989). These data are displayed in Figure 3, where the points represent 0.2-s integrations and the lines represent models that will be discussed below. The gradual drop of the light curve from the unocculted stellar signal is caused by Pluto's atmosphere. In the upper part of the light curve there may be one or two spikes, but the scarcity of these relative to giant planet occultation light curves indicates that Pluto's atmosphere is much more stable (fewer waves and/or turbulence) than the Jovian-planet atmospheres. The dashed line in Figure 3 shows a model isothermal atmosphere. The light curve follows the isothermal model until about half-intensity, and then it abruptly drops well below the isothermal model, which can be explained in two ways: (i) Pluto's atmosphere has a haze layer with a sharp upper boundary (Elliot et al. 1989; Elliot & Young 1992) whose extinction causes the light curve to abruptly drop; or (ii) Pluto's atmosphere has a thermal gradient (Eshleman 1989; Hubbard, Yelle, & Lunine 1990) strong enough (~20 K/km) to accomplish the same effect.

If we concentrate on the analysis of the upper, isothermal part of the light curve for the moment, Elliot & Young (1992) find T/μ for this part of the atmosphere to be 3.72 ± 0.75 (K/amu) and find a thermal gradient consistent with zero. Surface-ice spectroscopy by Owen et al (1993) detected N_2, CO, and CH_4, from which these authors concluded that the predominant constituent is N_2,

since it has by far the largest vapor pressure at the 40 ± 2 K temperature of Pluto's surface (Tryka et al. 1994).

The structure of Pluto's atmosphere as determined from the 1988 occultation is shown in Figure 4, where we have indicated the uncertainty in the lower part of the atmospheric structure that can be due to extinction or a sharp thermal gradient. This ambiguity could be resolved with future occultation observations, carried out simultaneously in the IR and visible with HOPI and SOFIA. Haze particles would be small and produce less extinction at IR wavelengths so the light curve would not drop as steeply. If the sharp drop is due to a thermal gradient, however, then the IR and optical light curves would appear nearly the same.

The model that describes the isothermal character of the upper part of the light curve, as established from the analysis of Elliot & Young (1992), was put forth by Yelle & Lunine (1989). Due to the large cross-sections of CH_4, it absorbs sunlight in the 3.3 μm band and then re-radiates in the 7.7 μm band, keeping the temperature at a nearly constant 102 K. Later Lellouch (1994) pointed out that CO cooling could be significant in the radiative transfer. Strobel et al (1996) have incorporated CO cooling into a more sophisticated model. However, these radiative transfer models have not yet demonstrated that they can generate temperature changes abrupt enough to explain the sharp drop in the light curve (Figure 3). Similarly, the haze interpretation of the sharp drop in the light curve suffers from no known mechanism to produce enough particles and keep them suspended (Stansberry et al. 1994).

Millis et al (1993) find a remarkable consistency among the temperatures of the isothermal part of the atmosphere and the radius of the "top of the haze" around the planet. Also, the surface radius deduced by Millis et al (1993, 1195 ± 5 km for the sharp-thermal-gradient assumption) is about 30-40 km larger than that deduced from the mutual events (Buie et al. 1992; Young & Binzel 1994). One explanation for this is that a deep troposphere could hide the surface from the occultation light curves, except for the more central stations (Stansberry et al. 1994).

Some models predict that Pluto's atmosphere will collapse as it recedes from the Sun, but this conclusion depends on the CH_4 fraction in Pluto's volatile reservoir (Trafton 1990). Stansberry (1996) points out that the alpha-beta phase transition for N_2 could buffer the atmosphere at the transition temperature and keep it from collapsing. Establishing how Pluto's atmosphere changes as it recedes from the sun could be carried out with a series of occultation observations with SOFIA.

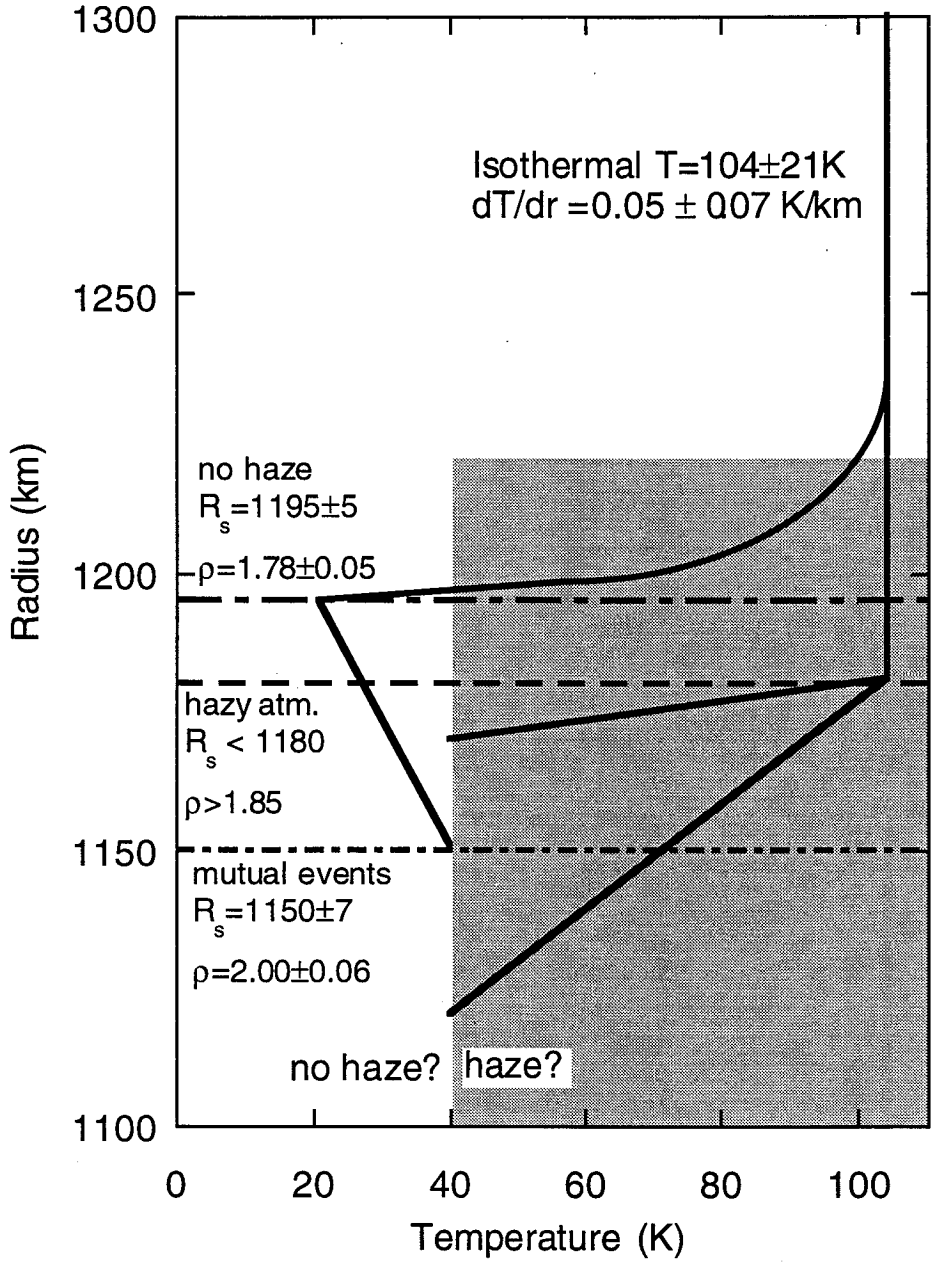

Figure 4. Structure of Pluto's atmosphere. The upper atmosphere is consistent with an isothermal temperature profile, while there are different possibilities for the lower atmosphere. A clear lower atmosphere requires a sharp thermal gradient and the observed surface radius from Millis et al (1993) of 1195 ± 5 km is consistent with the surface radius from the mutual events (Buie, Tholen, & Horne 1992) if a troposphere underlies the sharp thermal gradient (Stansberry et al. 1994) as depicted in the figure. The drop in the occultation light curve can also be explained by extinction and a thermal gradient (which may be more gradual). Two such profiles are shown. (Adapted from Elliot & Young 1992.)

PROPOSED OBJECTIVES

The objectives below may be achieved from the same occultations, depending on the particulars of the events. All Pluto occultation observations should be carried out as nearly as possible to a central chord, in order to probe most deeply into the atmosphere and to be able to use the central flash for accurate astrometry to determine the closest approach distance to the center of the shadow, should the troposphere model (Stansberry et al. 1996) correctly predict that the light-curve will become visible for central chords.

1) Determine whether a thermal gradient or a haze layer caused the sharp drop in the light curve we observed in 1988 by observation of an occultation with S/N ≥ 50 simultaneously in the visible and IR.

2) Detect or put a stringent upper limit on the variability of Pluto's atmospheric structure by probing it with a stellar occultation observation with S/N ≥ 50 once every 1-2 years.

3) Detect or limit non-isothermal structures in Pluto's atmosphere by observation of an occultation with a time resolution of 0.05 s.

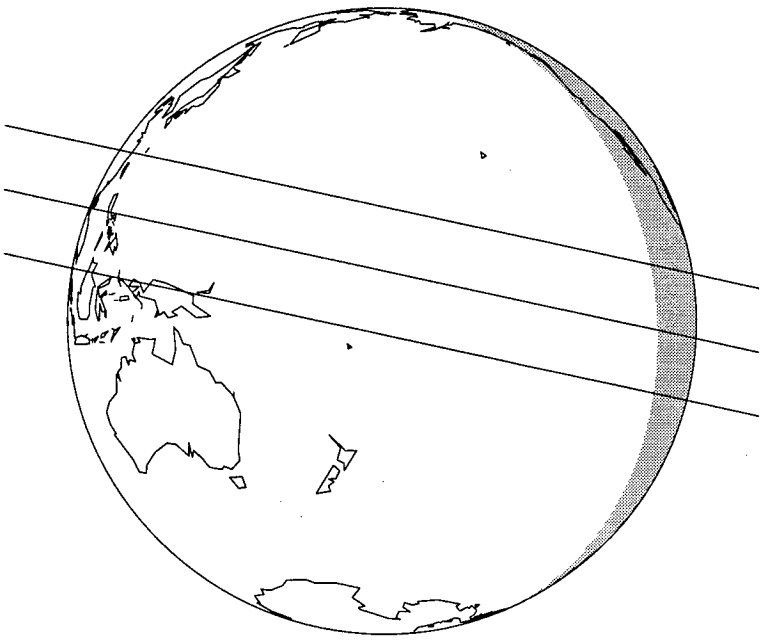

Fig. 5 Occultation of a 12.8 mag star by Pluto on November 11, 2002. The globe at the left shows a view of the Earth from Pluto when it occults a R = 12.8 mag star (McDonald, private communication). The centerline is the predicted center of Pluto's shadow, and the other two lines represent the limit of the northern and southern limbs. The shaded area is the region for which the sun is greater than 8 degrees below the horizon (Pluto is 33 deg from the sun). Both HOPI channels could obtain ~5 times the signal-to-noise of the light curve shown in Fig. 3 in the visible. Since the star is extremely red (B – R = 3.5), with simultaneous observations in the K band (with the facility IR camera, if it can record occultation data) we could obtain a light curve with comparable S/N. With these data we could answer the question of whether Pluto's atmosphere has a haze layer or sharp thermal gradient. Note that this event (if it follows the current prediction) would be easily accessible with SOFIA, but inaccessible from ground-based telescopes.

DOES CHARON HAVE AN ATMOSPHERE?

What is the smallest solar-system body that possesses a bound atmosphere? The ability of a body to hold an atmosphere depends on its surface gravity, distance from the sun, and its atmospheric gases. Being a satellite of Pluto, Charon's solar distance ranges from 30-50 au, and its surface gravity is about half that of Pluto. Presently the most sensitive Earth-based method for detecting an atmosphere of a distant body such as Charon is through stellar occultation observations, and in 1980 a stellar occultation by Charon was observed from Sutherland by Walker (1980). With these data he confirmed the existence of Charon as a satellite of Pluto, and his first order analysis placed a lower limit of 600 km on the radius of Charon. This lower limit lies above subsequent determinations of Charon's radius, 593 ± 20 km (Tholen and Buie 1988, 1989), from modeling of the series of mutual occultations and eclipses that have just been completed by Pluto and Charon (Binzel et al 1985).

Walker's original analysis did not consider a possible atmosphere and included several approximations at the 25 km level, so Elliot & Young (1991) reanalyzed the data with the goal of placing an upper limit on a possible atmosphere of Charon. They fit the stellar occultation data for Charon obtained by Walker (1980) with a model that included possible differential refraction by an atmosphere, followed by an abrupt occultation by Charon's limb. They found a lower limit (3σ, where σ = 0.8 km) on Charon's radius of 601.5 km, which can be used as a constraint for modeling the mutual event data. Although their model fits favored the possibility of a Charonian atmosphere (composition undetermined), the time resolution of the data is insufficient to be certain that an atmosphere has been detected. The data could also be interpreted as being indicative of (i) a slight extinction near Charon or (ii) an as yet unidentified effect, not associated with Charon. For the latter possibilities, they found an upper limit on a Charonian atmosphere of 1 to 57 cm-amagat, the exact amount depending on the gas assumed to be the major constituent.

Observations with higher time resolution and signal-to-noise than Walker's data could confirm or refute the possibility of an atmosphere on Charon.

PROPOSED OBJECTIVES

1) Detect or put an upper limit on its atmosphere 5 times more stringent that the present limit (Elliot & Young 1991) by observing an occultation with S/N ≥ 350.

2) Establish Charon's surface radius by observing an occultation with S/N ≥ 100. This S/N would allow detection of the Fresnel diffraction fringes from the limb that could be used to accurately set the closest approach distance between SOFIA and the center of the occultation shadow without need of a second occultation chord.

COMETS: DUST JETS AND COMA STRUCTURES

Many consider comets to be the "Rosetta stone" of solar-system formation, since these leftover building blocks of outer solar system bodies maintain a frozen record of chemical and physical processes that occurred over 4 billion years ago. Then not surprisingly, ESA has chosen "Rosetta" as the name of its mission to comet P/Wirtanen, where it will rendezvous in 2011 when the comet is near aphelion and will collect data through perihelion in 2013. This mission will feature two landers to sample the composition of the nucleus. Another way to learn the composition of cometary nuclei is by inference through studies of their emanations of gas and dust, driven by solar heating. Until recently, H_2O was considered the only volatile whose sublimation would drive dust from the surface of the nucleus. But some comets have exhibited outbursts too far from the sun for significant sublimation of H_2O, leading to the inference that these nuclei contain a significant amount of CO ice.

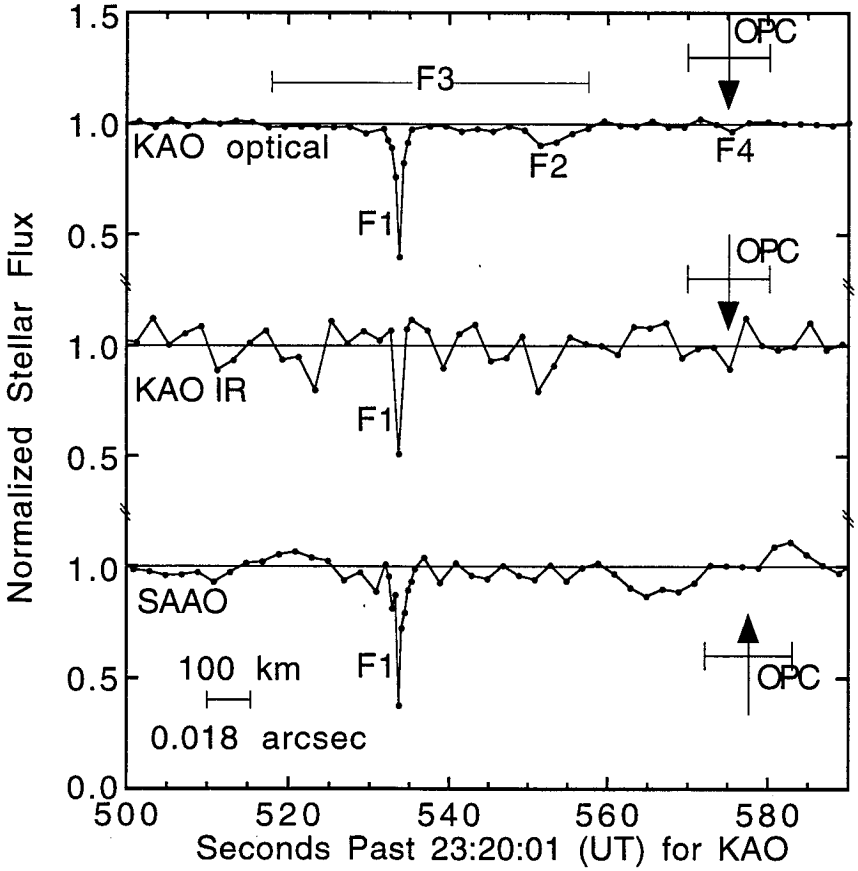

Figure 6. Chiron occultation light curves. Portions of the stellar flux (normalized to 1.0 for the unocculted star) from Ch08 have been plotted versus UT for an interval that includes Chiron's closest approach to Ch08. To enhance the signal-to-noise ratio, data outside of the sharp drop (F1) have been averaged to 2.0 s. The segment of the light curves comprising F1 have been left at full resolution for the KAO data, while the SAAO data have been averaged to 0.4 s (two integration times and two deadtimes). A sharp drop and recovery (F1) is evident in all three light curves. Since the paths of the KAO and SAAO were separated in Chiron's shadow plane by only 1.4 km at closest approach we have assumed that F1 was caused by the same material for both stations. Therefore, we corrected for the unknown timing offset in the SAAO data by retarding the time axis of the light curve by 309.9 s to align the sharp feature with that of the KAO. The features F1 and F2 are likely caused by dust jets, F3 is possibly the signature of a bound coma, and F4 (if real) would indicate material in the orbit plane of Chiron, since it occurs at the time when the star crossed the orbit plane (OPC). (after Elliot et al. 1995)

One of these bodies is the unusual object 2060 Chiron. Considered as a comet, Chiron is unusual in two respects: (i) it exhibits outbursts (Tholen, Hartmann, & Cruikshank 1988; Marcialis & Buratti 1993) at great distances from the sun (nearly up to its aphelion distance of 18.9 AU) (Bus et al. 1989), and (ii) its nucleus is much larger than any other known comet (Sykes & Walker 1991; Jewitt & Luu 1992). It is similar in size, however, to the Kuiper belt objects (Jewitt & Luu 1993), leading to the conjecture that Chiron is closely related to these objects, but its chaotic orbit (Scholl 1979) has brought it much closer to the sun. From the KAO we observed the first stellar occultation by Chiron simultaneously at visible and infrared wavelengths. We detected four features in the coma (Figure 6), with different degrees of certainty. Our conclusions about Chiron from this work and a previous stellar occultation (Buie 1993) are: (i) the jet-like features observed provide evidence that the coma material originates from just a few, small active areas, rather than uniform sublimation, (ii) a bound coma has possibly been detected, (iii) the particle radii in at least one of the jet-like features are larger than 0.25 μm, (iv) material in Chiron's orbit plane has likely been detected, and (v) the radius of Chiron's nucleus is in the range 83-156 km.

From the success of the Chiron observations, it is clear that stellar occultation studies can yield unique information, which would be particularly useful for comets being studied by other techniques as well, such as the Rosetta target comet, P/Wirtanen and P/Wild 4, the target for a recently approved Discovery mission that will return a sample of dust. Depending on the comet and the nature of the occultation opportunity, we can learn the structure of their comas at high spatial resolution, set lower limits on nuclear diameters, constrain particle size distributions of the dust and discover species that are more readily detected in absorption than in emission (the 4430 Å interstellar line, has not yet been detected in a comet).

PROPOSED OBJECTIVES

Our objectives for comet work concentrate on comets of particular interest, and all observations would be carried out simultaneously in the visible and IR in order to characterize the particle sizes in the dust.

1) Characterize the high-spatial resolution structure of the Rosetta target comet, P/Wirtanen through a series of occultation observations before, during, and after the Rosetta encounter.

2) Characterize the high-spatial resolution structure of the Discovery target comet, P/Wild 4 through a series of occultation observations before, during, and after the encounter.

3) Characterize the dust jets and other high-resolution structure in Chiron's coma at 1 au intervals as it recedes from the sun and at yearly intervals when the body is at aphelion.

KUIPER-BELT OBJECTS

As mentioned earlier, the Kuiper-belt objects are large, icy bodies (perhaps similar to Chiron) that orbit the sun beyond Neptune (Jewitt & Luu 1995). A fundamental property of these bodies yet to be determined are their diameters, which are needed to establish their albedos. For a body that is approximately spherical, its diameter can be learned from a multiple-chord stellar occultation. Alternatively, a single chord and the rate of passage of Fresnel diffraction fringes can be used to find the diameter.

Another goal would be to look for extinction by dust—indicative cometary activity in Kuiper-belt objects.

PROPOSED OBJECTIVES

Our objectives for Kuiper-Belt objects will require a factor of 5-10 improvement in our ability to predict occultations, since these bodies are thought to be similar in size to Chiron, but they are about 5 times more distant. Fortunately the signal-to-noise ratios depend on the magnitudes of the occulted stars, rather than the magnitudes of the Kuiper-Belt objects themselves!

1) Characterize possible cometary activity by searching for comas with stellar occultation observations with S/N $\geq$ 50-100.

2) Place lower limits on the radii of several bodies by observing stellar occultations with S/N ≥ 25; diameters can be determined if Fresnel fringes can be detected (S/N ≥ 100).

PLANETARY RINGS

Beginning with our discovery of the Uranian rings (Elliot, Dunham, & Mink 1977), occultations have been used to establish precise orbits of the Uranian and Saturnian ring systems (French et al. 1991; Elliot et al. 1993). In order to pin down ever more subtle dynamical effects involving ring precessions and particle-wave propagation, high S/N occultations should be continually observed. However, the large shadows of the ring systems usually cover one or more large telescopes on the Earth, so aircraft observations are generally not required. Exceptions to this are the ring arcs of Neptune and the Jovian ring (which never has a large opening angle); for these, the regions on Earth for useful observations can be small and contain no ground-based telescopes. In fact, in 1992, the shadow of a Neptune arc passed unobserved right between Palomar and Cerro Tololo (French et al. 1993)! Since observable occultations by Jupiter's and Neptune's rings are so rare, SOFIA observations may be the only way for us to make progress on understanding these systems.

PROPOSED OBJECTIVES

Our objectives for planetary rings are those for which an aircraft is necessary to be at a special location within the occultation shadow. Occultation observations would be carried out simultaneously in the visible and IR to constrain the sizes of the ring particles.

1) Characterize the structure of Neptune's ring-arcs versus longitude with occultations of opportunity.

2) Establish the albedo of the Jovian ring particles by observing an occultation with significantly greater S/N than our previous observations (Dunham et al. 1982).

III. THE NEED FOR AIRBORNE OBSERVATIONS

As demonstrated time and again by the KAO, an airborne observing platform provides several important advantages over ground-based observatories for occultations: (i) an aircraft can reach locations on Earth where an occultation is visible (which may not include any ground-based observatories); (ii) an aircraft can travel to the most advantageous location within the occultation shadow (usually as close as possible to the center); (iii) water-absorbed IR wavelengths are accessible; (iv) scintillation noise is much less; (v) the threat of clouds is virtually nil; and (vi) an aircraft can respond to last-minute updates in the predicted location of the occultation shadow path.

IV. HOPI OBSERVING PROGRAM

The Pluto occultation described in Figure 5 is an excellent way to kick off the SOFIA occultation program. It is the best Pluto event since the 1988 P8 event which resulted in the first detection of Pluto's atmosphere. With an S/N ratio five times greater, time resolution 10 times greater, the results will revolutionize our understanding of Pluto's atmospheric structure. Although it is sheer coincidence, it is interesting to note that observation of this event requires the 20° lower elevation limit that SOFIA provides. Not only is this event unobservable from any groundbased location, it would also be unobservable with the KAO, if it were still flying, because the telescope would not be able to point low enough in the sky.

We do not yet know what other occultation events will occur during the first two years of SOFIA operations, but the frequency of previous events suggests that we should expect that about 3-5 high-quality occultations per year should be observed with SOFIA and HOPI (some by us and some by Guest Investigators). We anticipate GI interest in ring events and also occultations by the atmospheres of the major planets. We also anticipate successful Guest Investigator programs involving high precision time resolved photometry for asteroseismology. The expected S/N ratio for such observations was marginal on the KAO, but SOFIA and HOPI will produce good results.

We also hope to participate in the initial test phase of SOFIA using our KAO experience and HOPI's capabilities to: 1) assess the telescope's pointing behavior over a wide range of frequencies; 2) measure the image quality across the focal plane in conjunction with the facililty IR camera; and 3) measure the in-flight optical alignment errors of the SOFIA telescope using a Shack-Hartmann test setup incorporated in HOPI. Our scientific program will profit from the best possible image quality with SOFIA, so we have an ongoing interest in improving and evaluating the performance of the telescope.

V. INSTRUMENT DESCRIPTION

Occultation astronomy places a number of unusual and stringent requirements on its observational instrumentation. First, time-resolved observations are needed with time resolution determined by the Fresnel zone size and the velocity of the shadow of the occulting object across the Earth. This requirement carries the important implication that use of longer integration times to increase the S/N ratio of an observation will simultaneously degrade the spatial resolution of the observation. The throughput of the system and the detector's read noise have an unalterable effect on the S/N ratio of a given occultation dataset. For occultations involving faint objects the critical factors are the quantum efficiency of the detector and its read noise, with the maximum possible read speed being determined by the overall sensitivity of the instrument. Second, it is critical to know the location of the observer and the time of the observation to high accuracy in order to allow several observations of the same event to be combined. Third, the physical processes involved in an occultation have wavelength dependence, and the S/N ratio of various events may be optimized at different wavelengths depending on the spectral class of the occulted star and the spectrum of the occulting object. This argues for an instrument capable of simultaneous observation at two or more different wavelengths. Fourth, every event is unique and cannot be reproduced so every effort must be made to record the highest quality and most reliable data. Airborne observations are, of course, of great assistance in this regard, but from an instrumentation point of view we have found that imaging data are far more reliable and of higher quality than aperture photometer data. The ability to use a reference star for point spread function fitting photometry greatly increases the S/N ratio, and the capability of looking at the actual images obtained makes detailed investigation of unexpected features in the light curve possible.

Our proposed instrument is called HOPI (High-Speed Occultation Photometer and Imager), and is a multichannel high-speed imaging photometer. Its anticipated performance relative to the fundamental requirements of occultation astronomy is shown in Table 1. The ideals given in Table 1 are derived from fundamental quantities such as the size of the Fresnel zone, typical occultation shadow velocities, obtainable S/N ratio as a function of wavelength, and the need for on-chip standard stars. A glance at this table shows that HOPI meets these ideals in every respect except 1) it lacks an IR channel; and 2) it does not have perfect throughput and zero noise.

Table 1 - Instrument Performance Summary

Requirement	Ideal Performance	HOPI Performance
Time Resolution	20 msec for 3 80"x80" subframes	20 msec for 3 80"x80" subframes
System throughput, Read noise	Unity Zero e^-/integration	See Figure 8 3 - 6 e^-/integration
Position/Time accuracy	30 meters / 1 msec	30 meters / 200 nsec (GPS)
Wavelength Range/Channels	0.3 - 4.0 μm / 3 channels	0.3 - 1.1 μm / 2 channels (excluding facility InSb camera)
Imaging Data	Yes	Yes
Multiple subframes	3 per detector	3 per detector

A fundamental change in the HOPI instrument concept resulted from the SOFIA Instrument Workshop when it became clear that there would be a facility IR camera whose requirements would nearly meet HOPI's IR requirements. *We propose to leave out the IR detector from HOPI at this time with the intent of using the facility instrument in concert with HOPI for those relatively rare events that have good S/N in the 2-5 μm region.* We propose to work closely with the UCLA group to insure that the facility camera will meet the time synchronization requirements of occultation work and that our two mechanical and optical configurations will allow simulaneous operation. This "descope" will save the project considerable effort and funds. Since this proposal does not include funding for development of the IR system, the remainder of the proposal will only discuss the two optical channels that now constitute the HOPI instrument. If, for some reason, it becomes clear that these two instruments cannot be made compatible, we will propose an alternative method to incorporate IR capability either with some other IR instrument or with a new one specifically made for the purpose if that is what is needed.

This proposal assumes that we will use an excellent commercial detector, the EEV CCD47-20, for HOPI. However, we are pursuing an additional avenue in an attempt to improve over the performance of this part. Please see the Technology Issues section for further details.

INSTRUMENT CONCEPT

The conceptual layout of HOPI is shown in Figure 7, with the optical path shown on the left and the data system on the right. These two major components of the instrument are discussed in the following two sections. Table 2 lists the most important specifications of the full HOPI system.

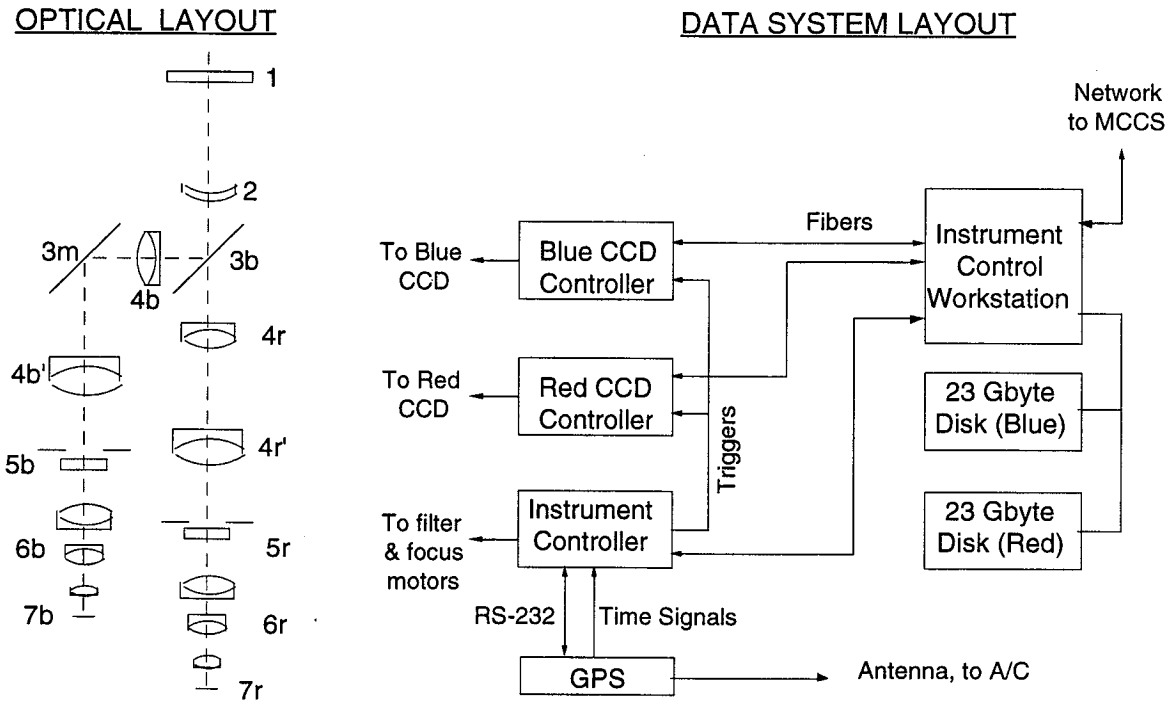

Figure 7. HOPI instrument concept. The HOPI optical layout is shown on the left with the data system block diagram on the right. Light enters the instrument through facility window 1 and is split by dichroic reflector 3b and folded by mirror 3m. Petzval collimators 4 form pupil images at stops 5 where filter wheels are also located. Camera lenses 6 reimage the focal plane on the blue CCD (7b) and red CCD (7r). The detectors are operated and read out by the CCD controllers with data from each detector routed through fiber optics to a single workstation which operates the entire system. The Instrument Controller is responsible for miscellaneous functions such as producing CCD trigger signals and operation of filter wheels and internal focus mechanisms.

Table 2 - Key HOPI System Specifications

Parameter	CCD Detector
SOFIA image size	4 arcsec for 80% enclosed light at optical wavelengths
Detector Organization	1Kx2K, frame transfer with split serial clocks & 2 amplifiers
Pixel Size	13μm, 1/3 arcsec on the sky (unbinned); operated binned 3x3 for occultations, unbinned for telescope testing.
Optical Reduction Factor	6.4:1
Field of View	Square FOV inscribed in the 8 arcmin diameter SOFIA field
Wavelength range	0.35-0.6 μm (blue channel) 0.6-1.0 μm (red channel)
Maximum Data Rate	4 Mbyte/sec, 16 bits/pixel for each CCD

OPTICAL SYSTEM AND DETECTORS:

Reimaging optics are essential to match the pixel size to the focal plane image size. Optical designs for similar systems (Persson et al 1992; Atwood et al 1992; Rayner et al 1993) and our own work during the HOPI study phase indicate that each of HOPI's optical channels will contain approximately 10 lenses in order to achieve satisfactory image quality. Good anti-reflection coatings can provide an optical throughput of 70% for this system including the dewar windows (Persson et al 1992). The optical design can be made with only one focal reduction ratio and different image scales can then be obtained by using on-chip binning. This is feasible because the proposed detectors can support high clocking rates and have a relatively large format. The reducing optics will provide an image scale of 1/3 arcecond per unbinned pixel. At this image scale, the diameter of the SOFIA field of view will equal the diagonal dimension of the CCD. For occultations the CCD will be binned 3x3 to produce 1 arcsecond binned pixels. This relieves the optical design and provides additional flexibility in changing the HOPI image scale.

The optical design work carried out during the study phase focused on a different detector that required both 10:1 and 3:1 focal reduction ratios. Late in the study period we became aware of the EEV detectors and will need to redo the optical design, which will be substantially simpler. It will also be necessary to develop the optical and mechanical design with consideration given to the interface with the facility IR camera.

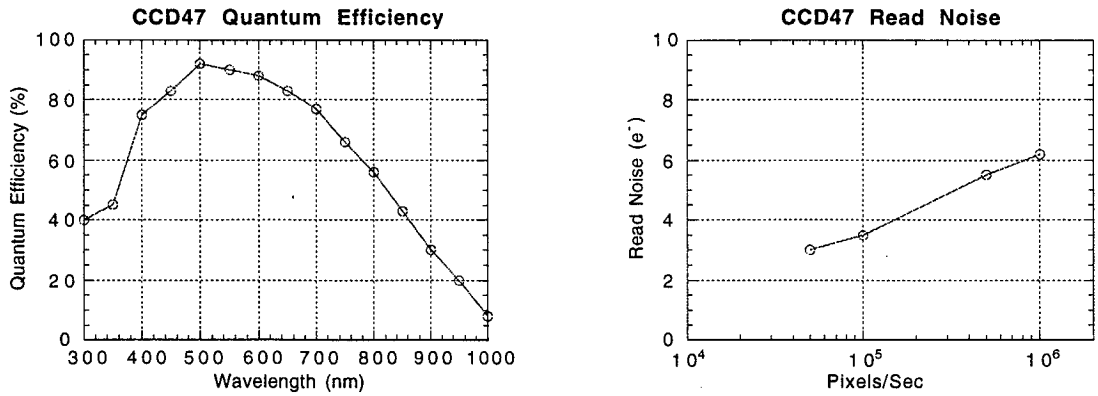

Figure 8. Measured QE of EEV CCD47-20 (left) and read noise as a function of read time for the EEV CCD47 amplifier (right). Data for both figures supplied by EEV.

The HOPI baseline CCDs are EEV CCD47-20's. These 1Kx2K frame-transfer devices have 13 μm square pixels and are thinned, back-illuminated, ion-implanted, and AR coated with Hafnium

Oxide. They have 2-stage amplifiers that provide relatively low read noise even at high read speeds. The measured QE curve and read noise as a function of readout speed, both supplied by EEV, are shown in Figure 8. If we are successful in our efforts to develop superior devices through our efforts with MIT Lincoln Labs, and as general progress is made on antireflection coatings for CCDs, these figures of merit will improve.

DATA SYSTEM

The HOPI data system layout is shown on the right side of Figure 7, and is based on the San Diego State University CCD controller (Leach & Denune 1994 Leach 1996, personal communication). The Generation II controller design is now available and can handle the high data rates we require, and is also capable of supporting the hardware timing functions demanded by occultation work. (Leach, 1996). For observations such as occultations of Kuiper belt objects, noise will be paramount and either a slower frame rate or smaller frame size can be chosen. For others, such as a central flash during an occultation by Jupiter, frame size and rate will be important and read noise will be negligible. HOPI will allow the tradeoff between speed and noise to be made for each observation.

Advances in computer capability in the last year have allowed us to simplify the proposed HOPI data system substantially during the study phase. The HOPI design is as modular as possible to realize the inherent redundancy present in a multichannel system and to maximize the system's flexibility. The data system hardware for each channel will be largely identical, the differences in operation being defined by software. The dewars, CCD controllers, and disk drives will be interchangeable. All connections between the rack and telescope will be fiber to eliminate grounding problems. The HOPI requirement for the facility cable drape will be three fiber pairs plus one spare pair, and a GPS antenna connection (RG59). The Instrument Control Workstation will be a Sun workstation, probably an Ultra 3 by the time we buy it, with two SDSU PCI interface cards installed. Both Sun and SDSU are migrating to the PCI interface standard for performance reasons, and by the time we procure the final computer system the PCI interface will likely be all that is available.

Single point failures can occur in the Instrument Controller, the Instrument Control Workstation, and the GPS clock unit. We propose to buy a GPS unit that is identical to those that we have used in our PCCD instrument and that were used on the KAO. This provides spares at no additional cost. The Instrument Controller will need to be made as inherently reliable as possible with board-level spares on hand. The weakest link is the Instrument Control Workstation. Machines of this kind are expensive enough and reliable enough that a true spare is not justified. Most failures will be reparable through normal computer maintenance and repair channels.

VI. ANTICIPATED PERFORMANCE

We now consider two different observational examples that illustrate HOPI's performance in occultation observing. The first case demonstrates the ultimate sensitivity of the system for a Triton occultation, and is illustrated in Figure 9. In this example, it is assumed that the integration time may be long (0.5 sec) and the dichroic beamsplitters have been removed. These assumptions allow a direct comparison between the PCCD and HOPI. Note that while the S/N ratio for the PCCD increases by the expected factor of three in going from the KAO to SOFIA, the HOPI S/N ratio is better than the PCCD's by another factor of two by virtue of its wider wavelength range and higher quantum efficiency. In addition, the S/N ratio for 0.5 second averages of HOPI data taken at a 50 ms integration time is shown. For the CCD this curve is nearly identical to the one for 0.5 second integrations, demonstrating that it is possible to operate in a regime limited by shot noise from the occulting object with 50 ms integrations. A similar curve for the PCCD does not exist, since it is incapable of operation at such fast frame rates.

For occulting objects much fainter than Triton, such as Kuiper belt objects, the observation would not be limited by shot noise from the occulting object. It would instead be read noise limited if observed at high speed (50 ms) and limited by shot noise on the sky at low speed (500 ms).

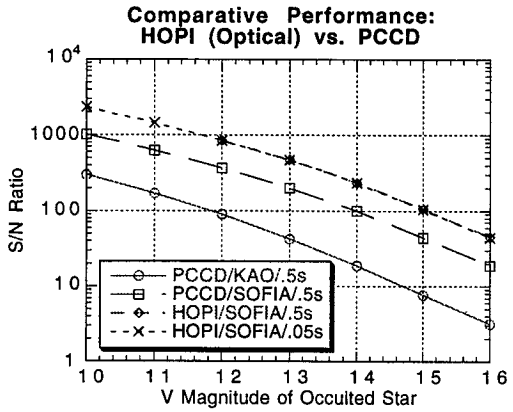

Figure 9. Ultimate sensitivity. In this example, Triton is the occulting body, and the integration time is slow. The dichroic beamsplitter is assumed to be removed to provide the best possible system throughput. In addition, no bandpass filter is used in the single optical channel . In this example, the limiting noise source is shot noise from Triton. For fainter occulting bodies, either read noise or shot noise on the sky would be the dominant noise source depending on the integration time. See text for further details.

While some of our scientific goals will require very high S/N lightcurves, most depend on simultaneous moderate S/N observations at two or three wavelengths. Our second example again uses a Triton occultation but with the two-channel HOPI configuration in place (see Figure 10). No filter is used in either the blue or red channels, so the system throughput as a function of wavelength defines the optical passbands. Read noise is again insignificant compared to shot noise on Triton so the S/N will scale with the square root of the integration time. If a gold dichroic reflector were added to allow use of an infrared channel, the S/N for the optical channels would drop by roughly the square root of 2 due to the light loss at the gold dichroic.

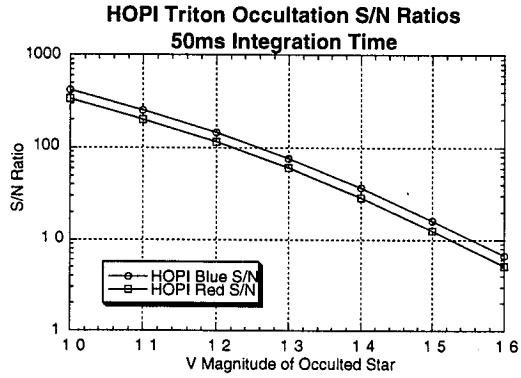

Figure 10. S/N ratios for Triton occultations observed with the two channel HOPI configuration for a 50ms integration time. The limiting noise source is again shot noise from Triton, so the S/N scales with the square root of the integration time.

In some cases it may be desirable to observe with narrow bandwidth filters, such as a 0.03 μm filter centered at the methane absorption band at 0.89 μm, in order to increase the contrast between the occulting object and the occulted star. In this case, read noise would be the dominant noise source.

SENSITIVITY CALCULATION

The determination of the ultimate sensitivity of an optical imaging system is quite straightforward. For a given SOFIA observation requiring a particular integration time and filter bandwidth, it depends on the read noise of the detector and the overall system throughput. Figure 8 shows the key detector figures of merit, read noise and quantum efficiency. The remaining important factor is the throughput of the instrument optics, which is estimated to be 70%.

Although it is possible to cast these sensitivity numbers (read noise, detector QE, and total system throughput) in the form of NEP and NEFD, the former quantities are generally used in optical astronomy rather than the latter ones.

VII. TECHNOLOGY ISSUES

The technoligies involved in HOPI are generally at, but not pressing, the state of the art. In the detector area HOPI may be able to extend the state of the art. We are proposing here to use EEV CCD 47-20 detectors, which at the time of this writing are not quite ready for commercial sale, but should be available in the early part of FY98. We have submitted a proposal to the MIT Lincoln Lab Advanced Concepts Committee to develop CCDs that have lower noise and higher speed than any commercial parts. If this is successful, we will be able to fly superior devices at no additional cost to SOFIA, but if not the EEV parts will still be very useful. Except for this possible development, HOPI will use commercial products in its development. Many parts will be custom made but will not require technology development for their fabrication to be successful.

VIII. REFERENCES

Atwood, B., Byard, P., DePoy, D. L., Frogel, J., & O'Brien, T. 1992, The Ohio State Infrared Imager/Spectrometer (OSIRIS)

Broadfoot, A. L. et al. 1989, Science 246, 1459

Buie, M. W. 1993, International Astronomical Union Circulars 5898

Buie, M. W., Tholen, D. J., & Horne, K. 1992, Icarus 97, 221

Bus, S. J., Bowell, E., Harris, A. W., & Hewitt, A. V. 1989, Icarus 77, 223

Cruikshank, D. P., Brown, R. H., Giver, L., & Tokunaga, A. T. 1989, Science 245, 283

Dunham, E., Elliot, J. L., Mink, D. J., & Klemola, A. R. 1982, AJ 87, 1423

Dunham, E. W. et al. 1995, BAAS 27, 1101

Elliot, J. L. et al. 1993, AJ 106, 2544

Elliot, J. L., Dunham, E., & Mink, D. 1977, Nature 267, 328

Elliot, J. L., Dunham, E. W., Bosh, A. S., Slivan, S. M., Young, L. A., Wasserman, L. H., & Millis, R. L. 1989, Icarus 77, 148

Elliot, J. L., Dunham, E. W., & Olkin, C. B. 1993, BAAS 25, 1106

Elliot, J. L., French, R. G., Dunham, E., Gierasch, P. J., Veverka, J., Church, C., & Sagan, C. 1977, ApJ 217, 661

Elliot, J. L. & Olkin, C. B. 1996, Probing Planetary Atmospheres with Stellar Occultations. In Annual Review of Earth and Planetary Sciences (ed. G. W. Wetherill), p. 89. Annual Reviews Inc., Palo Alto

Elliot, J. L. & Veverka, J. 1976, Icarus 27, 359

Elliot, J. L. & Young, L. A. 1991, Icarus 89, 244

Elliot, J. L. & Young, L. A. 1992, AJ 103, 991

Eshleman, V. R. 1989, Icarus 80, 439

French, R. G., Maene, S. A., Mason, E. C., McGhee, C. A., Nicholson, P. D., Matthews, K., & Roques, F. 1993, BAAS 25, 1110

French, R. G., Nicholson, P. D., Porco, C. C., & Marouf, E. A. 1991, Dynamics and structure of the Uranian rings. In Uranus (ed. J. T. Bergstralh, E. D. Miner, & M. S. Matthews), p. 327. University of Arizona Press, Tucson

Goldreich, P., Murray, N., Longaretti, P. Y., & Banfield, D. 1989, Science 245, 500

Halliday, I. 1965, S&T 29, 216

Hansen, C. J. & Paige, D. A. 1992, Icarus 99, 273

Hillier, J. & Veverka, J. 1994, Icarus 109, 284

Hubbard, W. B., Yelle, R. V., & Lunine, J. I. 1990, Icarus 84, 1

Ingersoll, A. P. & Tryka, K. A. 1990, Science 250, 435

Jewitt, D. & Luu, J. 1992, AJ 104, 398

Jewitt, D. & Luu, J. 1993, Nature 362, 730

Jewitt, D. C. & Luu, J. X. 1995, AJ 109, 1867

Leach, R. W. & Denune, J. 1994, Proc. S.P.I.E. 2198, 821

Leach, R. W. 1996, Proc. S.P.I.E. January, 1996. See also http://mintaka.sdsu.edu/ccdlab/

Lellouch, E. 1994, Icarus 108, 225

Marcialis, R. L. & Buratti, B. J. 1993, Icarus 104, 234

McKinnon, W. B. 1989, ApJL 344, L41

Millis, R. L. et al. 1993, Icarus 105, 282

Nicholson, P. D., McGhee, C., & French, R. G. 1995, Icarus 113, 57

Olkin, C. B., Elliot, J. L., Dunham, E. W., Millis, R. L., Wasserman, L. H., & Bus, S. J. 1993, BAAS 25, 1106

Olkin, C. B., Elliot, J. L., Hammel, H. B., Cooray, A., Foust, J. A., McDonald, S. W., & Dunham, E. W. 1995, BAAS 27, 1102
Olkin, C. B. et al. 1997, Icarus (in press)
Owen, T. C. et al. 1993, Science 261, 745
Persson, S. E., West, S. C., Carr, D. M., Sivaramakrishnan, A., & Murphy, D. C. 1992, PASP 104, 204
Rayner, J. et al. 1993, Proc. S.P.I.E. 1946, 490
Reitsema, H. J., Hubbard, W. B., Hill, R., Marcialis, R., & Howell, R. 1995, BAAS 27, 1101
Scholl, H. 1979, Icarus 40, 345
Smith, B. A. et al. 1989, Science 246, 1422
Soderblom, L. A. et al. 1990, Science 250, 410
Spencer, J. R., Buie, M. W., & Bjoraker, G. L. 1990, Icarus 88, 491
Spencer, J. R. & Moore, J. M. 1992, Icarus 99, 261
Stansberry, J. A., Lunine, J. I., Hubbard, W. B., Yelle, R. V., & Hunten, D. M. 1994, Icarus 111, 503
Stansberry, J. A., Pisaon, D. J., & Yelle, R. V. 1996, Planetary and Space Science In press.
Stansberry, J. A., Yelle, R. V., Lunine, J. I., & McEwen, A. S. 1992, Icarus 99, 242
Strobel, D. F. & Summers, M. E. 1995, Triton's upper atmosphere and ionosphere. In Neptune and Triton (ed. D. P. Cruikshank), p. 1107. University of Arizona Press, Tucson
Strobel, D. F., Zhu, X., Summers, M. E., & Stevens, M. H. 1996, Icarus 120, 266
Sykes, M. V. & Walker, R. G. 1991, Science 251, 777
Tholen, D. J., Hartmann, W. K., & Cruikshank, D. P. 1988, International Astronomical Union Circulars 4554
Trafton, L. 1990, ApJ 359, 512
Tryka, K. M., Brown, R. H., Cruikshank, D. P., Owen, T. C., Geballe, T. R., & DeBergh, C. 1994, Icarus 112, 513
Tyler, G. L. et al. 1989, Science 246, 1466
Wasserman, L. H., Buie, M. W., & Millis, R. L. 1995, BAAS 27, 1102
Yelle, R. V. & Lunine, J. I. 1989, Nature 339, 288
Yelle, R. V., Lunine, J. I., & Hunten, D. M. 1991, Icarus 89, 347
Yelle, R. V., Young, L. A., Vervack, R. J., Young, R., Pfister, L., & Sandel, B. R. 1996, JGR 101, 2149
Young, E. F. & Binzel, R. P. 1994, Icarus 108, 219